1352–1361 *Nucleic Acids Research, 2005, Vol. 33, No. 4*
doi:10.1093/nar/gki276

Mithramycin forms a stable dimeric complex by chelating with Fe(II): DNA-interacting characteristics, cellular permeation and cytotoxicity

Ming-Hon Hou[1,2,3] and Andrew H.-J. Wang[1,2,*]

[1]Institute of Biological Chemistry, Academia Sinica,Taipei, 115 Taiwan, [2]Institute of Biochemical Sciences, National Taiwan University, Taipei, 106 Taiwan and [3]Department of Food Science, Nutrition and Nutraceutical Biotechnology, Shih Chien University, Taipei, 104 Taiwan

Received December 28, 2004; Revised and Accepted February 10, 2005

ABSTRACT

Mith (mithramycin) forms a 2:1 stoichiometry drug–metal complex through the chelation with Fe(II) ion as studied using circular dichroism spectroscopy. The binding affinity between Mith and Fe(II) is much greater than other divalent metal ions, including Mg(II), Zn(II), Co(II), Ni(II) and Mn(II). The [$(Mith)_2$–Fe(II)] complex binds to DNA and induces a conformational change of DNA. Kinetic analysis of surface plasmon resonance studies revealed that the [$(Mith)_2$–Fe(II)] complex binds to DNA duplex with higher affinity compared with the [$(Mith)_2$–Mg(II)] complex. A molecular model of the Mith-DNA–Metal(II) complex is presented. DNA-break assay showed that the [$(Mith)_2$–Fe(II)] complex was capable of promoting the one-strand cleavage of plasmid DNA in the presence of hydrogen peroxide. Intracellular Fe(II) assays and fluorescence microscopy studies using K562 indicated that this dimer complex maintains its structural integrity and permeates into the inside of K562 cells, respectively. The [$(Mith)_2$–Fe(II)] complex exhibited higher cytotoxicity than the drug alone in some cancer cell lines, probably related to its higher DNA-binding and cleavage activity. Evidences obtained in this study suggest that the biological effects caused by the [$(Mith)_2$–Fe(II)] complex may be further explored in the future.

INTRODUCTION

The anticancer antibiotic mithramycin (plicamycin®) (Mith) belongs to the aureolic family isolated from *Streptomyces griseus* (1). Mith contains five sugar rings by using sugar residues A and C connected to an aglycon chromophore via O-glycosidic bonds, with the A–B disaccharide on one side and C–D–E trisaccharide on the other (Figure 1). This drug is a DNA-binding antitumor agent, which has been used clinically in several cancer therapies and Paget's disease (2–4). The antitumor property of Mith is probably associated with its inhibitory effects on replication and transcription of tumor cells (5,6). Recently, Fibach *et al*. (7) revealed that Mith could induce fetal hemoglobin production in normal and thalassemic human erythroid precursor cells, and suggested that Mith may be used as a therapeutic agent in certain neoplastic diseases.

Previous optical spectroscopy and footprinting studies revealed that Mith forms a dimer mediated by a single divalent metal ion, such as Mg(II) and Zn(II), which binds to DNA duplex around the GC-rich sequences that is at least 3 bp long (8–11). The structures of the metal-coordinated Mith dimer bound with DNA duplex have been analyzed using NMR by Patel and Shafer groups (12–14) who proposed that the binding of Mith to DNA leads the local structure into A-DNA conformation. Consequently, Mith may interfere with the transcription of genes that bear GC-rich motifs in their promoters, such as *c-myc* proto-oncogene (15).

Metal ions play an indispensable role in the actions of some synthetic and natural metalloantibiotics, and are involved in specific interactions of these antibiotics with biomolecules. A number of anticancer drugs complexed with metal ion are capable of inducing cancer cell death via DNA backbone cleavage (7). Some of these drugs are believed to be activated through a redox system, with the generation of hydroxyl free radicals. For example, pepleomycin (PEP) and bleomycin (BLM) belong to a class of important clinical anticancer drugs that cleave DNA at GpT or GpC sites. DNA degradation caused by PEP and BLM requires prior activation of the drug with molecular oxygen and certain metals ions, such as Fe(II) or Co(III). The close connection between DNA binding (or DNA damage) and inhibition of cell proliferation

*To whom correspondence should be addressed. Tel: +886 2 27881981; Fax: +886 2 27882043; Email: ahjwang@gate.sinica.edu.tw

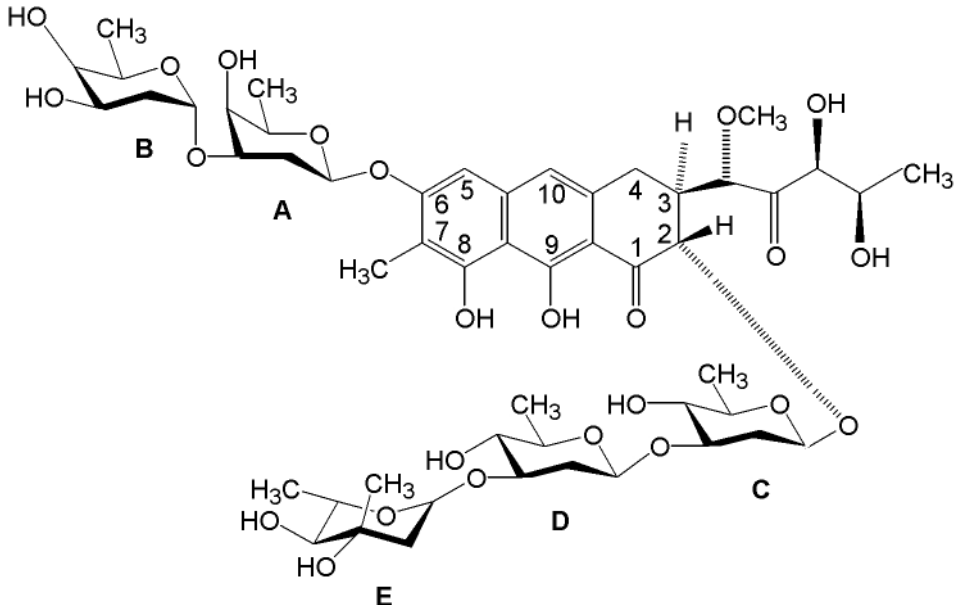

Figure 1. Chemical structure of mithramycin (Mith).

has suggested that Fe(II)–drug complexes with strong DNA-binding affinity are useful in the inhibition of tumor cell growth (7).

Mg(II)-coordinated Mith dimer was formed in the absence of DNA at concentrations of Mg(II) in the high-mM range (9). In addition to Mg(II), other divalent cations with radius <0.85 Å are candidates for promoting drug dimer formation as well (8,16). In this study, we investigated the ability of Mith to form a dimer complex in the presence of Fe(II) (and other metal ions) and its DNA-interacting property. The cleavage effects of the [$(Mith)_2$–Fe(II)] complex on DNA and the integrity and cellular permeation of the [$(Mith)_2$–Fe(II)] complex in cells were evaluated. Finally, the cytotoxicity of the stable [$(Mith)_2$–Fe(II)] complex toward cancer cell lines appeared to be higher than the drug alone, making it possible for the development of Fe(II) derivative of Mith as a potential target in the future.

MATERIALS AND METHODS

The synthetic DNA oligonucleotides were purified using gel electrophoresis. Mith was purchased from Sigma Chemical Co. (St Louis, MO). Absorbance measurements were carried out in a quartz cuvette using a Hitachi U-2000 spectrophotometer. The concentrations of Mith were estimated using extinction coefficients of 10 000 M^{-1} cm^{-1} at 400 nm. The concentrations of oligonucleotides were determined according to Beer's law ($A = \varepsilon bc$; where A is the optical density at 260 nm, ε is the extinction coefficient, b is the cell path length (1 cm) and c is the DNA concentration).

Molecular modeling

Molecular modeling was carried out on a Silicon Graphics workstation. Previous studies have shown that the Chro–DNA and Mith–DNA complexes have global similarities, as well as local differences (14,17). In addition, the coordination geometry surrounding the metal ion has been defined in the crystal structure of the [$(Chro)_2$–Mg(II)] complex bound to a DNA duplex. In this study, we use the Chro–DNA duplex crystal structure as a template to construct a plausible Mith–DNA complex by using the molecular modeling programs including Insight II and CNS. There are several differences between Chro and Mith, including the functional groups on sugar rings, sugar chirality and sugar–sugar linkages. Based on the [$(Mith)_2$–Mg(II)]-d$(TGGCCA)_2$ NMR structure, we modify the side chain of sugar, the A–B and D–E sugar linkages, as well as in the chirality of the E sugar of the initial model (14). Some distance restraints between Mith and DNA, obtained from the [$(Mith)_2$–Mg(II)]-d$(TGGCCA)_2$ NMR structure, were added to the refinement using the procedure implemented in CNS. The DNA force-field parameters of Parkinson *et al.* (18) were used. The quality of the model geometry was evaluated by r.m.s. derivation of bond length and bond angle.

CD experiments

The circular dichroism (CD) spectra were collected between 520 and 200 nm with bandwidth at 1 nm interval using a JASCO-720 CD spectropolarimeter. All spectra were the average of five runs. Method of CD spectral analysis was described previously (19). The data corresponding to the titration of Mith with metal (II) (normalized intensity change at λ_{275} versus metal concentrations) were fitted using a non-linear least squares plot. The evaluation of the dissociation equilibrium constant (K_d) between Mith and Metal(II) is measured as follows:

$$2\mathrm{Mith} + \mathrm{Metal(II)} \leftrightarrow (\mathrm{Mith})_2 \cdot \mathrm{Metal(II)}.$$

At equilibrium, the law of mass action gives:

$$K_d = [\mathrm{Mith}]^2[\mathrm{Metal(II)}]/\left[(\mathrm{Mith})_2 \cdot \mathrm{Metal(II)}\right]. \quad \mathbf{1}$$

The CD intensity change of the Mith (I) at λ_{275} can be written as

$$I = I_{max} \times 2\left[(\text{Mith})_2 \cdot \text{Metal(II)}\right]/[\text{Mith}]_0, \quad \mathbf{2}$$

where $[\text{Mith}]_0$ is the initial Mith concentration and I_{max} is the maximum CD intensity change at λ_{275} corresponding to 100% of the complex in solution. At equilibrium, the concentrations in molarity (M) of both Mith and metals in solution can be expressed as:

$$\begin{aligned}[\text{Mith}] &= [\text{Mith}]_0 - 2\left[(\text{Mith})_2 \cdot \text{Metal(II)}\right] \\ [\text{Metal}] &= [\text{Metal}]_i - \left[(\text{Mith})_2 \cdot \text{Metal(II)}\right],\end{aligned} \quad \mathbf{3}$$

where $[\text{Metal}]_i$ is the concentration of added metal ion(II) in solution. Therefore, the unit of K_d is M^2.

SPR-binding analysis

The affinity, association and dissociation between drug and DNA duplexes were measured in a BIAcore 3000A surface plasmon resonance (SPR) instrument (Pharmacia, Uppsala, Sweden) with a SensorChip SA5 from Pharmacia by monitoring the refractive index change of the sensor chip surface. These changes are generally assumed to be proportional to the mass of the molecules bound to the chip and recorded in resonance unit (RU). The 5′-biotin-labeled DNA hairpin, biotin-d(TTGGCCAATGTTTGGCCAA), purified by PAGE, was used in SPR (hairpin loop underlined). To control the amount of the DNA bound to the SA chip surface, the biotinated oligomer was immobilized manually onto the surface of a streptavidin chip until 1000 RU was reached. The Fe(II) derivative complex of Mith was prepared by the addition of Mith and $FeCl_2$ with a 2:1 ratio. Owing to the lower chelating affinity between Mith and Mg(II), the Mg(II) derivative complex of Mith was prepared by maintaining Mith in the constant concentration of 20 mM $MgCl_2$ in the binding process of SPR experiment. According to the recommendation of product information for SPR, the buffer (20 mM sodium-cacodylate) used in CD studies was replaced by 30 mM Tris–HCl buffered solution at pH 7.3 in the presence of 50 mM NaCl. Different concentrations of complexes were passed over the chip surface for 180 s at a flow rate of 10 μl min^{-1} to reach the equilibrium, and kept one of the flow cells blank as a control. The blank buffer solution was then passed over the chip to initiate the dissociation reaction and this was continued for 300 s to complete the reaction. After 300 s, the surface was recovered by washing with 10 μl of 10 mM HCl. Analysis of SPR-binding constant was described previously (19). Sensorgrams for the interactions between hairpin DNA duplex and drug were analyzed using BIA evaluation software version 3.

Measurement of DNA strand breakage and cell culture

The measurement of DNA strand breakage was performed according to the procedures reported previously with minor modifications (20). *Escherichia coli* was transformed with pET-21b and grown in Luria–Bertani medium. Plasmid DNA was then purified using Qiagen plasmid purification kit. Reagents were added in the following order: sterilized water, Mith (1, 10 and 50 μM), $FeCl_2$ (10 μM), H_2O_2 (1 mM) and supercoiled plasmid DNA (3 μg ml^{-1}). Samples were incubated at room temperature for 30 min before electrophoresis in a 1% agarose gel at 3 V cm^{-1} and stained with ethidium bromide for analysis. The intensity of DNA conformation was evaluated using ImageMaster (Pharmacia). All cell lines were obtained from the American Type Culture Collection (Rockville, MD). The human K562 erythroleukemia cells were grown in RPMI-1640 medium supplemented with 10% fetal bovine serum, glucose, L-glutamine and antibiotics. The other cell lines, including the human hepatoblastoma cell lines (HepG2 and Hep3B) and the human breast cancer cell line (MCF-7), were grown in the DMEM containing the same supplements as those described for RPMI-1640. All cells were maintained in a 5% CO_2 atmosphere at 37°C.

Fluorescence studies for intracellular free Fe(II) and visualization of drug localization within cells

The fluorescence probe (Calcein-AM; Sigma) used for intracellular-free Fe(II) detection was described previously (21–23). The human erythroleukemia K562 cell lines were loaded at a density of 5×10^6 cells ml^{-1} with 0.2 μM calcein-AM for 5 min at 37°C in RPMI medium without serum, washed twice to remove excess calcein-AM by phosphate-buffered saline (PBS) and finally, resuspended in RPMI-1640 medium until use. Just prior to measurement, 1.5 ml calcein-loaded cell suspension was centrifuged, followed by resuspension of cells in Tris-buffered salt solution, which contained 1.5 ml of pre-warmed, 150 mM NaCl, 5 mM KCl, 20 mM Tris and 5.5 mM glucose, adjusted to pH 7.3. The cell suspension was transferred into a stirred, thermostated cuvette at 37°C, and then fluorescence measurement initiated. Calcein fluorescence (excitation at 488 nm; emission at 510 nm) was measured in a fluorimeter equipped with a temperature-controlled cuvette holder and magnetic stirrer. Free Fe(II) contents were determined from the slopes of calcein fluorescence quenching traces. The K562 cells were incubated in RPMI-1640 for 1 h with the complex prepared from the 10 μM Mith in the presence of $FeCl_2$ with the metal/drug ratio of 2:1 for 4 h. Cells were then washed twice using PBS for 5 min each time after which the cells on chamber slide were visualized at green fluorescence under a fluorescence microscope.

Cell viability assay

Cellular proliferations were evaluated using the WST-1 assay kit (Roche, NJ). The assay is based on the ability of viable cells to reduce soluble yellow tetrazolium salt to dark red formazan crystals. The cells were seeded into 96-well plates. The drug complex was dissolved in the medium described above and added to the cell solutions covering a range of concentrations (0–10 μM). After 24–48 h, 10 μl of WST-1 dye was added and the plates were incubated in a moist chamber at 37°C for another 3 h. Optical density was measured at 470 nm on an ELISA reader. At least two independent measurements in each experiment were performed.

RESULTS

Interactions of Mith with divalent metal ions

In order to characterize the conformational change of the optically active Mith in the presence of divalent cations, the shift was monitored using CD spectra. Figure 2A shows

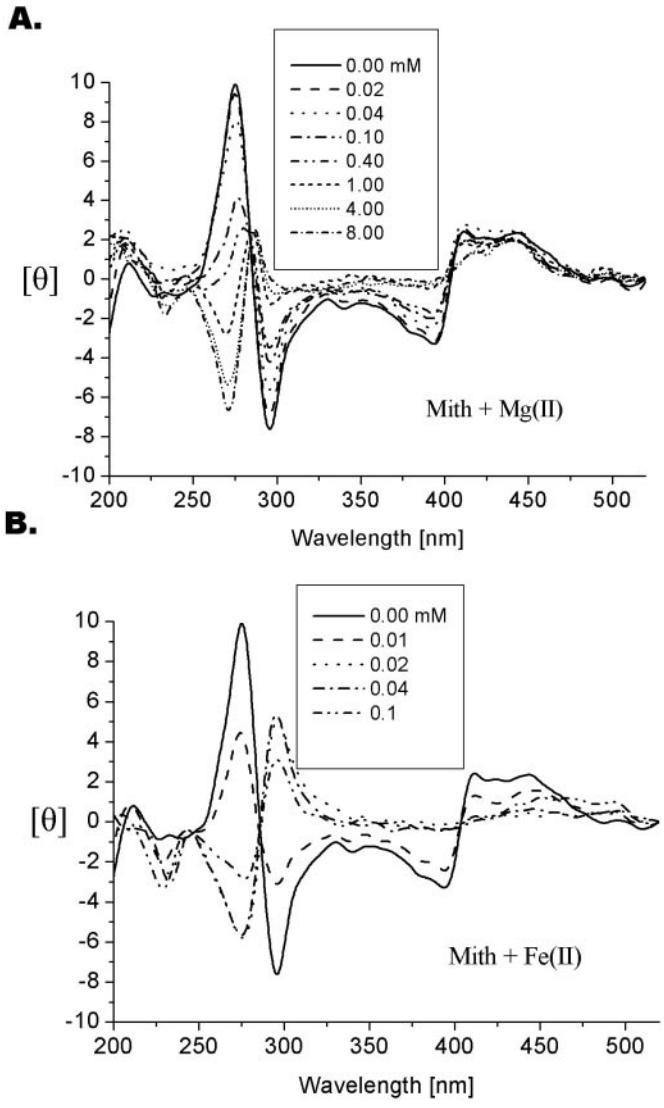

Figure 2. CD spectra of (**A**) Mith in the presence of Mg(II) with concentrations varying from 0 to 8 mM at 25°C (bottom). CD spectra of (**B**) Mith in the presence of Fe(II) with concentration varying from 0 to 0.1 mM (bottom) at 25°C. The drug concentration is 40 μM, buffered by 20 mM sodium-cacodylate at pH 7.3. The two isobestic points at 285 and 402 nm remain basically unchanged between the two complexes' association with Mg(II) and Fe(II) ions.

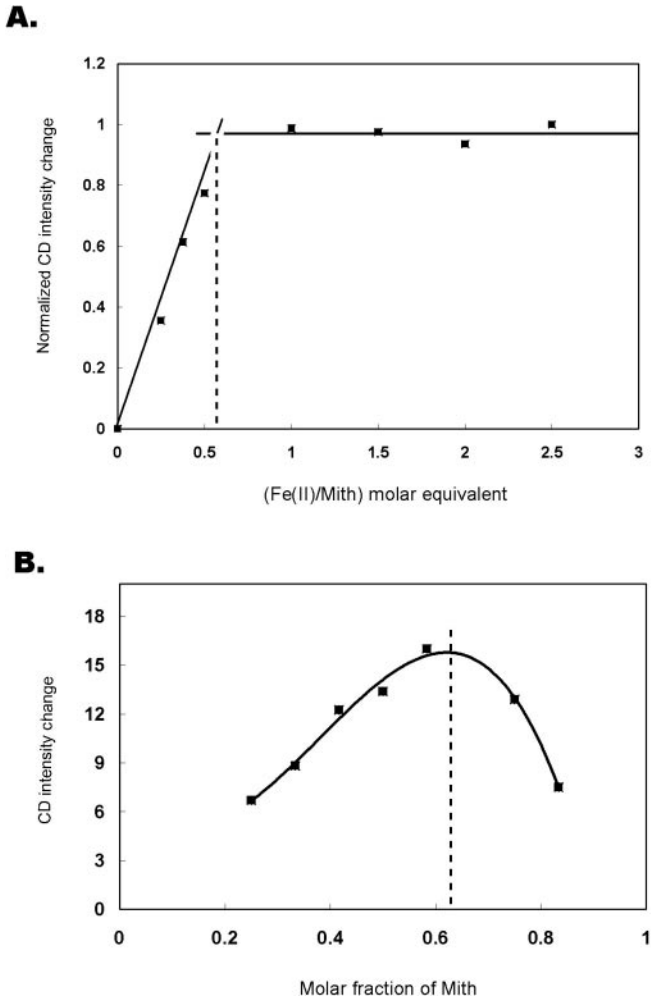

Figure 3. (**A**) CD titration of Mith against Fe(II) with normalized CD intensities change at 275 nm versus molar equivalents of [Fe(II)–Mith] at 25°C. The drug concentration is 40 μM, buffered by 20 mM sodium-cacodylate at pH 7.3. The two dashed lines in the figure represent the initial binding curve of Fe(II) to mithramycin and the one reaching the plateau. (**B**) Job-type titration plots for Fe(II)–Mith in 20 mM sodium-cacodylate at pH 7.3 at 25°C. The total concentration of Mith and metal was set at 60 μM.

the CD spectra (520–220 nm) of Mith upon the addition of Mg(II). These changes of CD spectra are associated with the concomitant decreased positive and negative peak intensities at 413 and 400 nm in the visible region, respectively. The occurrence of two isobestic points at 285 and 402 nm remaining basically unchanged demonstrates the presence of one-mode conformation alternation of Mith by binding with Mg(II). The feature in the 250–300 nm region arises from absorption assigned to the aglycon chromophore ring of the free Mith and is polarized along the long axis (24,25). However, the spectral changes were particularly pronounced in the UV region, with decreased negative peak intensity at 300 nm, with an ultimate inversion of the band in the 250–300 nm region at high concentration of Mg(II) ion. This result shows that the electronic transition of chromophore was changed by metal ion and suggests that the metal ion may coordinate with the oxygen atoms of the each chromophore ring of Mith. These distinctive features of the CD spectra owing to the chiral dimer formation of Mith are consistent with the earlier reports using CD spectra (9,26).

The metal-binding cavity of the $(Mith)_2$–metal ion complex was shown to have well-defined dimensions, accommodating only cations of ionic radius <0.85 Å (16). In this study, we tested the binding of several metal ions with Mith. Figure 2B shows the CD spectral changes of Mith upon the addition of Fe(II) in addition to the changes of CD spectra with the concomitant decreased positive and negative peak intensities at 413 and 400 nm in the visible region, respectively. The positive peak at 450 nm and the negative peak at 300 nm have obviously diminished and have inverted by the addition of Fe(II). The inversion of the band at 275 nm region was observed during the formation of the Mith–Fe(II) complex. These features are similar to those from the titration of Mg(II). A plot of the intensity of the signal at 275 nm against the concentration of added Fe(II) showed that a plateau

was reached when ~0.5 equivalent of Fe(II) had been added (Figure 3A). In addition, Job-type titration for Fe(II) was also performed at 275 nm using CD spectra at 25°C. The mole fraction between Fe(II) and Mith was varied (i.e. 0.0–1.0 mol equiv.). The data of Job-type titration plot showed a distinctive maximum at ~0.65 (mole fraction of Mith), confirming the 2:1 stoichiometry (Figure 3B). These results demonstrate the formation of the complex of Mith dimer chelated with Fe(II).

The changes in CD spectra between dimer and monomer of Mith in the presence of several other metal ions, including Zn(II), Co(II), Ni(II) and Mn(II), were also measured (Supplementary Figure 1S). The features of the spectral changes from monomer to dimer caused by some divalent ions are also similar to those caused by Fe(II). The spectral shape of the dimer complex contains an inversion of a band in the 250–280 nm region compared with that of drug alone. A previous study has shown that the dissociation equilibrium constant (K_d) between Mith dimer and Mg(II) calculated by absorption spectra was 3.96×10^{-8} M^2 (26). In order to compare the chelating specificity of various divalent metal ions with Mith, we carried out titration studies using CD spectra (metal concentrations versus normalized intensity change at λ_{275}) and calculated the K_d of the formation of the drug dimer. The isobestic points of CD spectra demonstrate the monomer–dimer interconversion on Mith by binding with Metal(II) ion. The distinctive feature of inversion of the band at 275 nm served as a marker for the dimer formation of Mith at differernt concentration of Metal(II) ion. The evaluation of K_d between Mith and Mith(II) was described in Materials and Methods. In the present study, the K_d values of the [$(Mith)_2$–Metal(II)] complexes determined using CD spectra were 1.14×10^{-8}, 1.29×10^{-8}, 7.41×10^{-10}, 3.99×10^{-9}, 1.54×10^{-10} and 5.03×10^{-11} M^2 for Mg(II), Mn(II), Co(II), Zn(II), Ni(II) and Fe(II), respectively. Here, our results show that Mith has higher binding affinity and specificity toward Fe(II) than any other divalent ions tested here.

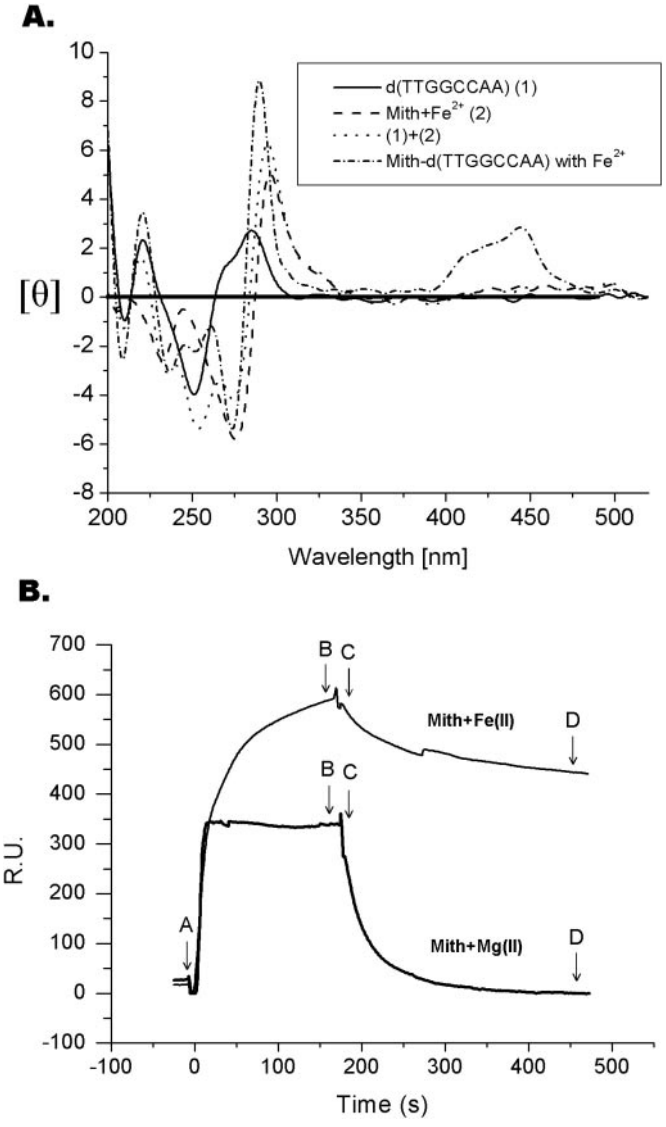

Figure 4. (**A**) Comparison of the CD spectra of the [$(Mith)_2$–Fe(II)] complex, $d(TTGGCCAA)_2$, [$(Mith)_2$–Fe(II)]-$d(TTGGCCAA)_2$ complex and the sum of the CD spectra of [$(Mith)_2$–Fe(II)] plus $d(TTGGCCAA)_2$ in 20 mM sodium-cacodylate buffer at pH 7.3 with 100 mM NaCl at 25°C. (**B**) Sensorgram of Mith–DNA interaction between immobilized hairpin DNA duplex and the target [$(Mith)_2$–Fe(II)] and [$(Mith)_2$–Mg(II)] complexes by subtracting the reference of control. The concentration of each target is 10 μM, in 50 mM NaCl, buffered by 30 mM Tris–HCl (pH 7.3) at 20°C. The start (A) and end (B) point of the association and the start (C) and end (D) point of the dissociation are indicated by arrows.

Interaction of the [$(Mith)_2$–Fe(II)] complex to $d(TTGGCCAA)_2$

We characterized the structural effects of the [$(Mith)_2$–Fe(II)] complex on the conformation change of $d(TTGGCCAA)_2$ DNA duplex using CD analyses. Figure 4A shows the CD spectra of various species. The CD spectra of the [$(Mith)_2$–Fe(II)] complex exhibit negative and positive peak intensities at 275 and 300 nm. In addition, the CD spectra of $d(TTGGCCAA)_2$ have a band with negative and positive peaks around 250 and 280 nm, typical of B-DNA. These results showed that the CD spectra of Mith and DNA signals overlap in the 200–300 nm regions. In this study, we compare the CD spectra of [$(Mith)_2$–Fe(II)]-$d(TTGGCCAA)_2$ complex with the normalized sum of the CD spectra of the [$(Mith)_2$–Fe(II)] complex plus $d(TTGGCCAA)_2$. The induced CD intensity changes at 287 and 275 nm, resulting from a strong exciton-type couplet, are used as evidence for the relative binding affinities of the [$(Mith)_2$–Fe(II)] complex toward this DNA oligomer duplex. In addition, the visible region of CD spectra can also serve as gauges for the conformation of Mith dimer complex. Our study has shown that the positive peak at 450 nm was diminished by the addition of Fe(II) without DNA duplex. However, the positive peak at 450 nm appeared upon the addition of $d(TTGGCCAA)_2$ (8).

Interaction of the [$(Mith)_2$–Fe(II)] complex with hairpin DNA using SPR

In order to study the effects of Fe(II) and Mg(II) on the binding affinity of DNA–Mith interaction, the maximum binding capacity (R_{max}) (in RU) was measured using SPR in the presence of Fe(II) and Mg(II). To ensure the formation of the DNA duplex at flowed SPR system, the biotin-labeled hairpin DNA duplex providing one Mith DNA-binding site (GGCC) was used as the probe. In Figure 4B, the [$(Mith)_2$–Fe(II)] complex appears to

be a better species than the [(Mith)$_2$–Mg(II)] complex in terms of the maximum binding capacity between drug and DNA duplex (~595 RU versus ~345 RU). With the increase in RU at the association phase (denoted A to B), the [(Mith)$_2$–Mg(II)] complex binds to DNA duplex more rapidly than [(Mith)$_2$–Fe(II)] and reaches a stable steady-state plateau. However, at the dissociation phase, the reduction of RU shows that the [(Mith)$_2$–Fe(II)] complex dissociates from DNA duplex more slowly as compared with the [(Mith)$_2$-Mg(II)] complex (denoted C to D). The kinetic experiments were carried out by measuring the binding parameter between the Mith and its target DNA duplex. The rate constants of association (k_a) and dissociation (k_d), calculated according to Materials and Methods section, are shown in Table 1. The [(Mith)$_2$–Fe(II)] complex binds to DNA duplex with the lower k_a and k_d compared with the [(Mith)$_2$–Mg(II)] complex. So the stabilizing effect on the association and dissociation of DNA–Mith interaction is dependent on the type of cations(II). According to the equilibrium constants data, the K_a of [(Mith)$_2$–Fe(II)] complex was elevated significantly (10-fold higher) than the [(Mith)$_2$–Mg(II)] complex. Thus, [(Mith)$_2$–Fe(II)] interacts with DNA duplex with higher affinity than [(Mith)$_2$–Mg(II)].

Effects of Mith on Fe(II)-mediated DNA cleavage in plasmid DNA

DNA cleavage converts the supercoiled circular form of DNA plasmid into relaxed open circular (OC) form and linear (L) form. If one strand is cleaved, the supercoils will relax to produce an OC form. If both strands are cleaved, L form DNA will be generated and it migrates between the supercoiled circular (SC) form and the OC form. In the plasmid DNA integrity studies, we examined the effect of Mith on Fe(II)-mediated DNA strand scission in plasmid DNA (Figure 5). Untreated plasmid was observed on gels as a single supercoiled (SC) DNA band. When plasmid DNA was treated with Fe(II) and H_2O_2, SC DNA was partially converted into the OC form. The redox-active [EDTA–Fe(II)] complex was used as a control, owing to its well-characterized properties, and the results are the same as the previous studies (20).

As shown in Figure 5, comparing with the control, at Mith/iron ratios of 0.1, 1 and 5, Mith increased the band intensity of the OC form DNA to 1.5-, 5- and 10-fold, respectively. The Mith–Fe(II) complex seems to process DNA cleavage and the SC plasmid appears to be converted into more OC form DNA products through single strand cleavage events when the Mith/Fe(II) ratio increased. In addition, a small amount of band intensity of L form DNA was observed at Mith/iron ratios of 1 and 5, suggesting that two nicked sites caused by the Mith–Fe(II) complex in different DNA strands are very close leading to the appearance of the L form DNA.

Table 1. Binding parameters between Mith dimer complex and hairpin DNA in the presence of Mg(II) and Fe(II) determined by SPR

Dimer form	k_a (M^{-1} s^{-1})[a]	k_d (s^{-1})[a]	K^a (M^{-1})[b]
(Mith)$_2$–Fe(II)	0.37×10^3	7.55×10^{-4}	4.9×10^5
(Mith)$_2$–Mg(II)	1.6×10^3	2.86×10^{-2}	0.56×10^5

[a]Typical error for the k_a and k_d values are 20 and 10%, respectively.
[b]K_a value obtained from k_a divided by k_d.

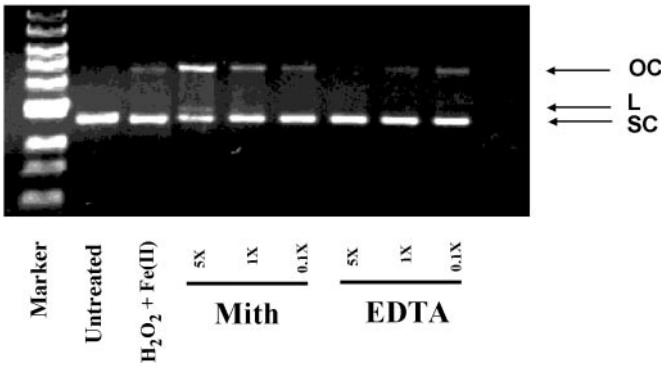

Figure 5. The effects of EDTA and Mith on integrity of the supercoiled plasmid DNA (pET-21b) when incubated in the presence of Fe(II) and hydrogen peroxide. The ratios of drugs versus Fe(II) are represented as 5×, 1× and 0.1× for 5:1, 1:1 and 1:10, respectively. The assays were carried out as described in Materials and Methods.

Assessing the chelating stability of Mith to Fe(II) in K562 cells

We showed that Mith formed a stable dimeric complex with Fe(II) at micromolar concentration with higher binding affinity in buffer solution. In order to examine the chelating ability of Mith with Fe(II) in cells, we have utilized a fluorescence sensor, calcein-AM, to probe the free Fe(II) contents in human erythroleukemia K562 cells. As shown in Figure 6A, the fluorescence of K562 cells loaded with calcein-AM showed a time-dependent decrease upon exposure to 20 μM Fe(II), suggesting that this decrease reflects the interaction of Fe(II) with calcein. This result showed that calcein fluorescence probe is located intracellularly and Fe(II) must cross the plasma membrane to quench it. However, when the calcein-loaded K562 cells were exposed to the [(Mith)$_2$–Fe(II)] complex, the fluorescent signals remain unchanged. These results suggest that Mith chelate with Fe(II) strongly in dimer forms, and they do not dissociate to release free Fe(II) ion in cellular cytosol.

The cellular permeation of Mith complex was investigated using fluorescence microscopy. We treated K562 cells with 10 μM [(Mith)$_2$–Fe(II)] complex. Figure 6B shows that the Mith complex concentrates in the nuclear compartment rather than the cytoplasm. These results provide strong evidence that the complex is membrane permeable. Together, these results indicate that the dimer complex maintains its chemical structural integrity and the Fe(II) ion cannot be released into cells.

Sensitivity of the [(Mith)$_2$–Fe(II)] complex treated cancer cell lines

The above results show that Fe(II) was capable of promoting the dimer formation of Mith in solution and in cells very effectively. In order to evaluate the cytotoxicity of the dimer–Fe(II) complex, the ability of the [(Mith)$_2$–Fe(II)] complex to inhibit cellular proliferation was assessed in hepatoma HepG2 and Hep3B cells by WST assay. The activity was compared with Mith alone as controls.

Table 2 shows the IC_{50} values of HepG2 and Hep3B when incubated with Mith at 24 and 48 h in the absence and presence of Fe(II) (5 μM). Cell growth was inhibited in both cell lines. Hep3B cells appeared to be more sensitive to Mith, as

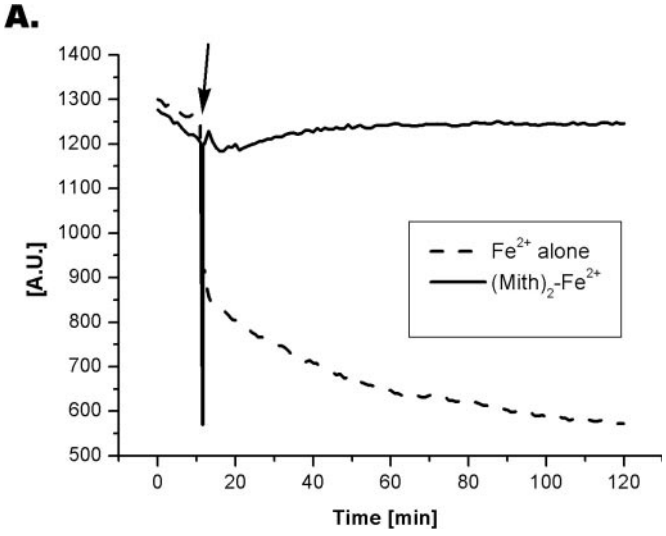

Figure 6. (**A**) The effect of the [(Mith)$_2$–Fe(II)] complex on calcein-detectable cellular Fe(II) content. The fluorescence of calcein-loaded K562 cells were treated with two different compounds as denoted by arrows, including 30 μM $FeCl_2$ (control), and 10 μM [(Mith)$_2$–Fe(II)] complex, buffered by PBS buffer at pH 7.3. (**B**) Subcellular locations of the [(Mith)$_2$–Fe(II)] complex are detected by phase contrast (left) and fluorescence (right) microscope. The location of cell nucleus was indicated by arrows.

Table 2. IC_{50} (μM) of Mith and the (Mith)$_2$–Fe(II) complex in various cancer cell lines at 24 and 48 h

Cell line type	Mith		(Mith)$_2$–Fe(II)	
	24 h	48 h	24 h	48 h
HepG2	>10	10 (±2)	>10	1 (±0.2)
Hep3B	1 (±0.2)	0.1 (±0.02)	0.4 (±0.1)	0.1 (±0.03)
K562	>10	0.3 (±0.1)	5 (±0.3)	0.1 (±0.05)
MCF-7	>10	0.4 (±0.1)	>10	0.35 (±0.1)

IC_{50} indicates 50% inhibitory concentration.

compared with HepG2 cells. Treatment of both cell lines for 48 h with 10 μM $FeCl_2$ alone did not visibly affect the cell viability. However, Fe(II) was shown to potentiate the anti-proliferation effects of Mith to HepG2 at 48 h with the IC_{50} value being 1 μM. These values are 10-fold better compared with those of Mith treatment alone at 48 h. Moreover, Fe(II) increased the cytotoxicity to Hep3B in response to Mith, visible even at 24 h (Supplementary Figure 2S). Hence, Fe(II) enhanced the cytotoxic activity of Mith against HepG2 and Hep3B cells through the formed dimer. We also tested the cytotoxicity of the [(Mith)$_2$–Fe(II)] complex toward other cell lines. The viability of K562 erythroleukemia cells and MCF-7 breast cancer cells were assessed under the same conditions as described for HepG2 and Hep3B cell lines. Table 2 shows the IC_{50} values of K562 and MCF-7 cancer cells incubated with Mith at 24 and 48 h in the absence and presence of Fe(II). Mith in the presence of Fe(II) was shown to be more active to K562 cells with IC_{50} values being 5 and 0.1 μM at 24 and 48 h, respectively, than Mith alone. Although no significant effect after either 24 h or 48 h exposure was seen in MCF-7 cancer cells, the [(Mith)$_2$–Fe(II)] complex maintained its cytotoxicity comparable to free Mith.

DISCUSSION

Although most antibiotics do not need metal ions for their biological activity, some, such as BLM, PEP and Mith, require metal ion to function properly. The coordinated metal ions play an important role in maintaining the proper structure or function of those antibiotics. Recently, the use of the aureolic family drugs is re-emerging (27,28). Mith has been administered clinically as free compound without other additive such as metal ions. This drug is believed to act by binding to DNA, which requires a metal-chelated form of dimeric drug complex.

Earlier studies focused on the interactions between Mith and Mg(II), which form two types of complexes with different stoichiometries and formation constants depending upon the concentration of Mg(II) (8,26). Recently, the dimer structure of Chro (a Mith analog) without DNA has been solved and showed that Metal(II) adopts an octahedral coordination by binding to O1 and O9 atoms of two independent chromophore and two water (Supplementary Figure 3S) (A.H.-J. Wang, H. Robinson, Y.G. Gao and M.-H. Hou, unpublished data). Mutual stacking of the aromatic ring of the chromophore of one monomer with the C–D glycosidic linkage of the other monomer provides stability for dimer formation. Here, our results showed that Mith was converted into a dimer in the presence of Fe(II) at near stoichiometry 2:1 ratio between the drugs and Fe(II) even at micromolar concentration using CD titration studies. In addition to CD spectra, Job-type titration plot of absorption spectra also confirm the 2:1 stoichiometry between Mith and Fe(II) (Supplementary Figure 4S). The stoichiometry of the Mith–Fe(II) complex is similar to some specific iron chelators commonly used in cancer therapy (29,30). Previous NMR and spectroscopic studies have shown that Mith appeared to have metal cation selectivity (13). For example, Demicheli *et al*. (31) have shown that Zn(II) is more efficient than Mg(II) in promoting dimer formation of Mith. Moreover, the metal binding cavity was shown to have well-defined dimensions accommodating only divalent cations of ionic radius <0.85 Å (16). The radius of Fe(II) is 0.76 Å, fulfilling this requirement. Mith has a much higher affinity toward Fe(II) than any other metals, such as Mg(II), Co(II), Mn(II), Ni(II) and Zn(II). Furthermore, the conformation of Mith dimer chelated with Fe(II) is similar to that of Mith dimer chelated with Mg(II).

In order to examine the chelating ability of Mith with Fe(II) in cells, we have utilized a fluorescence sensor, calcein, which can be easily loaded into cells to probe the integrity for the [(Mith)$_2$–Fe(II)] complex. Some of the calceins bind intracellular iron, yielding the fluorescence-quenched calcein–Fe(II).

The changes in calcein fluorescence provided a means for on-line tracing of cytosolic iron levels in living cells, used for the monitoring of iron transport, chelator action or intracellular release or sequestration of iron under a variety of experimental conditions (32,33). Interestingly, our studies showed that the fluorescence intensity of calcein remains constant while treating with the [$(Mith)_2$–Fe(II)] complex, showing that the [$(Mith)_2$–Fe(II)] complex did not dissociate to release free Fe(II) ion and form calcein–Fe(II), and this complex remained dimeric conformation in cellular cytosol. Additionally, visualization of [$(Mith)_2$–Fe(II)] by fluorescence microscopy shows that this dimer complex is capable of traversing the cytoplasmic membrane and accumulating inside of cells.

CD analysis, a good indicator for DNA conformational change, has been used to measure the conformation change during the [$(Mith)_2$–Fe(II)] complex binding (34). The CD intensities in 287 and 275 nm (UV region) are induced by the binding of [$(Mith)_2$–Fe(II)] complex toward this DNA oligomer duplex, and the characteristic feature of CD spectra resembles to that of the [$(Mith)_2$–Mg(II)] complex in the presence of DNA duplex. According to this result, no significant difference was observed in DNA conformation change by binding with Mith dimer chelated with Fe(II) or Mg(II). Although the solution structures of the Metal(II)-coordinated Mith–DNA complex have been analyzed using NMR spectroscopy (12–14), the precise coordination geometry

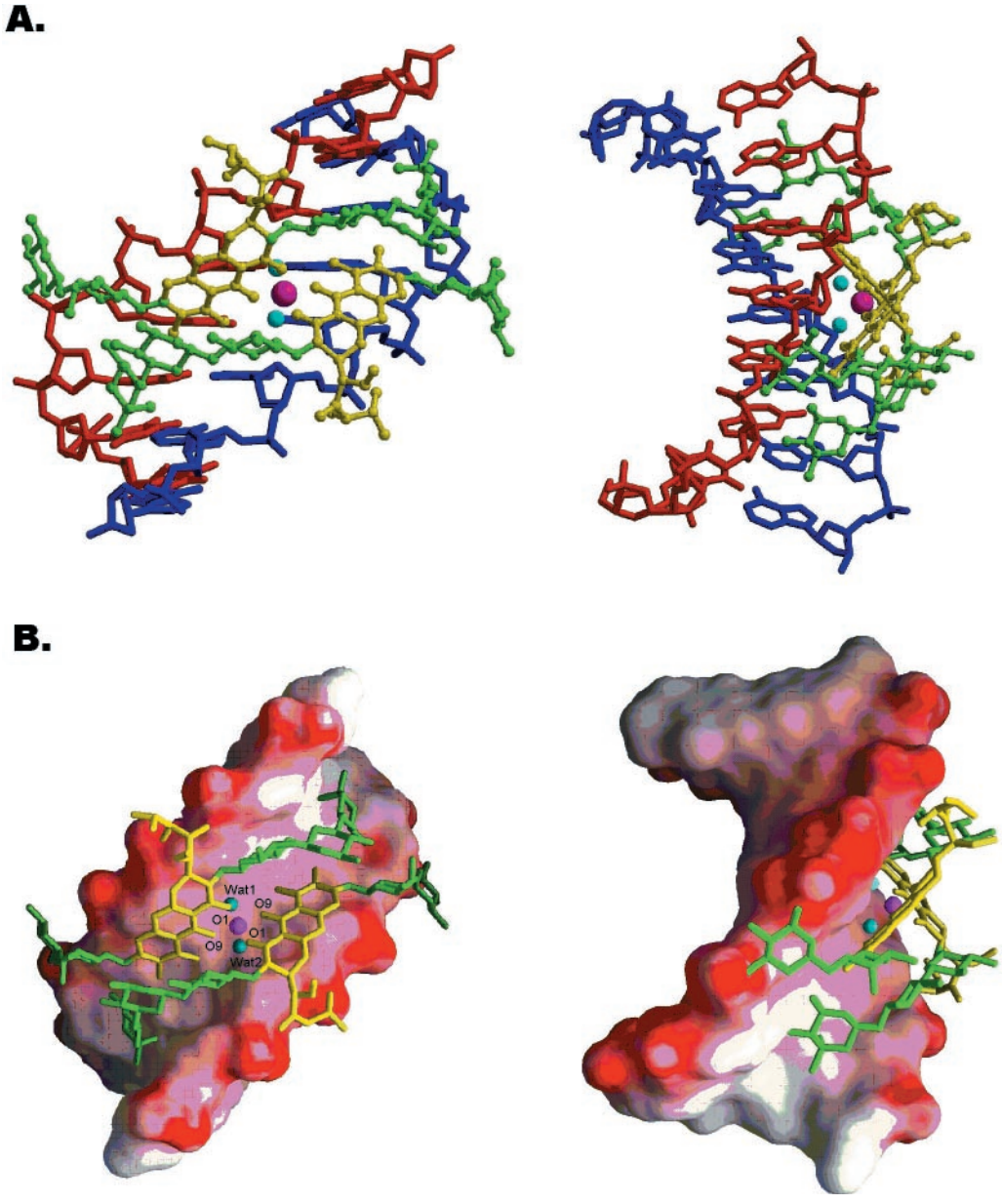

Figure 7. (**A**) The drawings of the metal(II)-coordinated [Mith-$(TTGGCCAA)]_2$ model viewed from the minor groove (left) and backbone direction, Mith containing chromophore (yellow) and saccharide (green) in ball and stick, and DNA in skeletal line drawing. (**B**) Surface representation of the metal(II)-coordinated [Mith-$(TTGGCCAA)]_2$ model shown with DNA electrostatic potentials viewed from the minor groove (left) and backbone (right). The metal(II) and waters are depicted in pink and blue, respectively.

around the metal ion remains unclear. Recently, the coordination geometry surrounding the metal ion was unequivocally defined in our X-ray crystallographic studies of the [$(Chro)_2$–Mg(II)] complex bound to a DNA duplex (17). In this study, we propose a model of Mith bound to $d(TTGGCCAA)_2$ duplex. Basically, the NMR structure of Mith bound to $d(TGGCCA)_2$ duplex and the model of Mith bound to $d(TTGGCCAA)_2$ duplex show global similarities and local differences. The model reveals the octahedral coordination around the metal ion which binds to O1 and O9 atoms of the two chromophores and two water molecules act as the fifth and sixth ligands (Figure 7A and B). This is different from that of the NMR structure, which showed a tetrahedral coordination geometry around the metal ion.

The binding constants between Mith and DNA have been measured previously (8,35). Aich and Dasgupta (8) have shown that the association equilibrium constant (K_a) of Mith bound to calf thymus DNA is $\sim 1.15 \times 10^5\ M^{-1}$ in the presence of Mg(II). The recent development of biosensor technologies for biospecific interaction analysis enables monitoring of a variety of molecular reactions in real-time using SPR (36,37). In this study, we demonstrate that molecular interactions between DNA-binding drug (Mith) and biotinylated target DNA probes immobilized on sensor chips is detectable by SPR technology using a commercially available biosensor. In principle, the self-complementary d(TTGGCCAA) provides one DNA-binding site for Mith according to our CD and modeling study. Considering the low stability and dissociation character of oligonucleotide duplex (octamer) at flowed SPR system, the part of loop (TGT) in hairpin DNA was used to ensure the formation of the self-complementary d(TTGGCCAA) duplex in binding and regeneration process. The analysis of the kinetic parameters reveals marked differences between the [$(Mith)_2$–Fe(II)] and [$(Mith)_2$–Mg(II)] complex interacting with DNA duplex. Not only the [$(Mith)_2$–Fe(II)] complex exhibits the slower rates of association and dissociation, but also the binding affinity of [$(Mith)_2$–Fe(II)] interacting with the DNA duplex is 10 times higher than that of [$(Mith)_2$–Mg(II)].

Some metal ions and complexes can undergo one-electron redox reactions (such as copper, iron or manganese) producing reactive oxygen species, the latter then damage DNA, frequently yielding strand breaks (38). In this study, our results proposed that the [$(Mith)_2$–Fe(II)] complex promotes one-strand DNA scission DNA by producing reactive hydroxyl radicals in the presence of H_2O_2 (Figure 5). However, the mechanism remains to be elucidated. It would be interesting to study the DNA cleavage mechanism of the [$(Mith)_2$–Fe(II)] complex in the future. The preferred binding sites for mithramycin on different DNA fragments have been investigated by DNAase footprinting assay (11,39). Previous studies showed that Mith is a well-known GC-rich DNA-binding drug, suggesting that the [$(Mith)_2$–Fe(II)] complex may have GC cleavage specificity.

In the early studies, complexes of the structurally related DNA-binding anticancer antibiotics with metals have been tested in order to amplify their potential in cancer therapy by Fiallo *et al.* (40). For example, doxorubicin, one of the best known anticancer drugs, has been tested regarding its mode of complexation with a number of metal ions such as Pt(II), Fe(III) and Cu(II) on the effects of tumor cells (41). This study has identified that the coordination of Mith with Fe(II) ion could enhance the cytotoxicity of the drug against some cancer cell lines and suggested a new anticancer mechanism of Mith.

SUPPLEMENTARY MATERIAL

Supplementary Material is available at NAR Online.

ACKNOWLEDGEMENTS

We thank Dr L.S. Kan for assistance in this study. This work was supported by Academia Sinica to A.H.-J.W. M.H.H. was supported by a postdoctoral fellowship from Academia Sinica. Funding to pay the Open Access publication charges for this article was provided by Academia Sinica.

REFERENCES

1. Slavik,M. and Carter,S.K. (1975) Chromomycin A_3, mithramycin, and olivomycin: antitumor antibiotics of related structure. *Adv. Pharmacol. Chemother.*, **12**, 1–30.
2. Kennedy,B.J. (1972) Mithramycin therapy in testicular cancer. *J. Urol.*, **107**, 429–432.
3. Du Priest,R.W.,Jr and Fletcher,W.S. (1973) Chemotherapy of testicular germinal tumors. *Oncology*, **28**, 147–163.
4. Elias,E.G. and Evans,J.T. (1972) Mithramycin in the treatment of Paget's disease of bone. *J. Bone Joint Surg. Am.*, **54**, 1730–1736.
5. Goldberg,I.H. and Friedman,P.A. (1971) Antibiotics and nucleic acids. *Annu. Rev. Biochem.*, **40**, 775–810.
6. Yang,X.L. and Wang,A.H.-J. (1999) Structural studies of atom-specific anticancer drugs acting on DNA. *Pharmacol. Ther.*, **83**, 181–215.
7. Fibach,E., Bianchi,N., Borgatti,M., Prus,E. and Gambari,R. (2003) Mithramycin induces fetal hemoglobin production in normal and thalassemic human erythroid precursor cells. *Blood*, **102**, 1276–1281.
8. Aich,P. and Dasgupta,D. (1995) Role of magnesium ion in mithramycin–DNA interaction: binding of mithramycin–Mg^{2+} complexes with DNA. *Biochemistry*, **34**, 1376–1385.
9. Cons,B.M. and Fox,K.R. (1989) Interaction of mithramycin with metal ions and DNA. *Biochem. Biophys. Res. Commun.*, **160**, 517–524.
10. Keniry,M.A., Banville,D.L., Simmonds,P.M. and Shafer,R. (1993) Nuclear magnetic resonance comparison of the binding sites of mithramycin and chromomycin on the self-complementary oligonucleotide $d(ACCCGGGT)_2$. Evidence that the saccharide chains have a role in sequence specificity. *J. Mol. Biol.*, **231**, 753–767.
11. Fox,K.R. and Howarth,N.R. (1985) Investigations into the sequence-selective binding of mithramycin and related ligands to DNA. *Nucleic Acids Res.*, **13**, 8695–8714.
12. Keniry,M.A., Owen,E.A. and Shafer,R.H. (2000) The three-dimensional structure of the 4:1 mithramycin:$d(ACCCGGGT)_2$ complex: evidence for an interaction between the E saccharides. *Biopolymers*, **54**, 104–114.
13. Sastry,M., Fiala,R. and Patel,D.J. (1995) Solution structure of mithramycin dimers bound to partially overlapping sites on DNA. *J. Mol. Biol.*, **251**, 674–689.
14. Sastry,M. and Patel,D.J. (1993) Solution structure of the mithramycin dimer–DNA complex. *Biochemistry*, **32**, 6588–6604.
15. Jones,D.E.,Jr, Cui,D.M. and Miller,D.M. (1995) Expression of beta-galactosidase under the control of the human c-myc promoter in transgenic mice is inhibited by mithramycin. *Oncogene*, **10**, 2323–2330.
16. Itzhaki,L., Weinberger,S., Livnah,N. and Berman,E. (1990) A unique binding cavity for divalent cations in the DNA–metal–chromomycin A_3 complex. *Biopolymers*, **29**, 481–489.
17. Hou,M.H., Robinson,H., Gao,Y.G. and Wang,A.H.-J (2004) Crystal structure of the [Mg^{2+}–(chromomycin $A_3)_2$]-$d(TTGGCCAA)_2$ complex reveals GGCC binding specificity of the drug dimer chelated by a metal ion. *Nucleic Acids Res.*, **32**, 2214–2222.
18. Parkinson,G., Vojtechovsky,J., Clowney,L., Brunger,A.T. and Berman,H.M. (1996) New parameters for the refinement of nucleic acid containing structures. *Acta Crystallogr. D*, **52**, 57–64.

19. Hou,M.H., Lin,S.B., Yuann,J.M., Lin,W.C., Wang,A.H.-J. and Kan,L.S. (2001) Effects of polyamines on the thermal stability and formation kinetics of DNA duplexes with abnormal structure. *Nucleic Acids Res*., **29**, 5121–5128.
20. Lovejoy,D.B. and Richardson,D.R. (2002) Novel ''hybrid'' iron chelators derived from aroylhydrazones and thiosemicarbazones demonstrate selective antiproliferative activity against tumor cells. *Blood*, **100**, 666–676.
21. Breuer,W., Epsztejn,S., Millgram,P. and Cabantchik,I.Z. (1995) Transport of iron and other transition metals into cells as revealed by a fluorescent probe. *Am. J. Physiol*., **268**, C1354–C1361.
22. Breuer,W., Epsztejn,S. and Cabantchik,Z.I. (1995) Iron acquired from transferrin by K562 cells is delivered into a cytoplasmic pool of chelatable iron(II). *J. Biol. Chem.*, **270**, 24209–24215.
23. Cabantchik,Z.I., Glickstein,H., Milgram,P. and Breuer,W. (1996) A fluorescence assay for assessing chelation of intracellular iron in a membrane model system and in mammalian cells. *Anal. Biochem*., **233**, 221–227.
24. Cons,B.M. and Fox,K.R. (1990) The GC-selective ligand mithramycin alters the structure of $(AT)_n$ sequences flanking its binding sites. *FEBS Lett*., **264**, 100–104.
25. Huang,H.W., Li,D. and Cowan,J.A. (1995) Biostructural chemistry of magnesium. Regulation of mithramycin–DNA interactions by Mg^{2+} coordination. *Biochimie*, **77**, 729–738.
26. Aich,P. and Dasgupta,D. (1990) Role of Mg^{++} in the mithramycin–DNA interaction: evidence for two types of mithramycin–Mg^{++} complex. *Biochem. Biophys. Res. Commun*., **173**, 689–696.
27. Remsing,L.L., Gonzalez,A.M., Nur-e-Alam,M., Fernandez-Lozano,M.J., Brana,A.F., Rix,U., Oliveira,M.A., Mendez,C., Salas,J.A. and Rohr,J. (2003) Mithramycin SK, a novel antitumor drug with improved therapeutic index, mithramycin SA, and demycarosyl-mithramycin SK: three new products generated in the mithramycin producer *Streptomyces argillaceus* through combinatorial biosynthesis. *J. Am. Chem. Soc*., **125**, 5745–5753.
28. Ferrante,R.J., Ryu,H., Kubilus,J.K., D'Mello,S., Sugars,K.L., Lee,J., Lu,P., Smith,K., Browne,S., Beal,M.F. *et al*. (2004) Chemotherapy for the brain: the antitumor antibiotic mithramycin prolongs survival in a mouse model of Huntington's disease. *J. Neurosci*., **24**, 10335–10342.
29. Gao,J. and Richardson,D.R. (2001) The potential of iron chelators of the pyridoxal isonicotinoyl hydrazone class as effective antiproliferative agents, IV: the mechanisms involved in inhibiting cell-cycle progression. *Blood*, **98**, 842–850.
30. Torti,S.V., Torti,F.M., Whitman,S.P., Brechbiel,M.W., Park,G. and Planalp,R.P. (1998) Tumor cell cytotoxicity of a novel metal chelator. *Blood*, **92**, 1384–1389.
31. Demicheli,C., Albertini,J.P. and Garnier-Suillerot,A. (1991) Interaction of mithramycin with DNA. Evidence that mithramycin binds to DNA as a dimer in a right-handed screw conformation. *Eur. J. Biochem*., **198**, 333–338.
32. Kakhlon,O. and Cabantchik,Z.I. (2002) The labile iron pool: characterization, measurement, and participation in cellular processes(1). *Free Radic. Biol. Med*., **33**, 1037–1046.
33. Konijn,A.M., Glickstein,H., Vaisman,B., Meyron-Holtz,E.G., Slotki,I.N. and Cabantchik,Z.I. (1999) The cellular labile iron pool and intracellular ferritin in K562 cells. *Blood*, **94**, 2128–2134.
34. Hou,M.H., Robinson,H., Gao,Y.G. and Wang,A.H.-J. (2002) Crystal structure of actinomycin D bound to the CTG triplet repeat sequences linked to neurological diseases. *Nucleic Acids Res*., **30**, 4910–4917.
35. Majee,S., Sen,R., Guha,S., Bhattacharyya,D. and Dasgupta,D. (1997) Differential interactions of the Mg^{2+} complexes of chromomycin A_3 and mithramycin with poly(dG–dC)×poly(dC–dG) and poly(dG)×poly(dC). *Biochemistry*, **36**, 2291–2299.
36. Carrasco,C., Joubert,A., Tardy,C., Maestre,N., Cacho,M., Brana,M.F. and Bailly,C. (2003) DNA sequence recognition by bispyrazino-naphthalimides antitumor agents. *Biochemistry*, **42**, 11751–11761.
37. Lacy,E.R., Nguyen,B., Le,M., Cox,K.K., OHare,C., Hartley,J.A., Lee,M. and Wilson,W.D. (2004) Energetic basis for selective recognition of TG mismatched base pairs in DNA by imidazole-rich polyamides. *Nucleic Acids Res*., **32**, 2000–2007.
38. Ming,L.J. (2003) Structure and function of ''metalloantibiotics''. *Med. Res. Rev*., **23**, 697–762.
39. Van Dyke,M.W. and Dervan,P.B. (1983) Chromomycin, mithramycin, and olivomycin binding sites on heterogeneous deoxyribonucleic acid. Footprinting with (methidiumpropyl-EDTA)iron(II). *Biochemistry*, **22**, 2373–2377.
40. Fiallo,M.M., Deydier,E., Bracci,M., Garnier-Suillerot,A. and Halvorsen,K. (2003) Mitomycin antitumor compounds. 2. Interaction of transition metal ions with mitomycin C. Solution structure and biological activity of a Pd^{2+}–MMC complex. *J. Med. Chem*., **46**, 1683–1689.
41. Fiallo,M.M., Drechsel,H., Garnier-Suillerot,A., Matzanke,B.F. and Kozlowski,H. (1999) Solution structure of iron(III)–anthracycline complexes. *J. Med. Chem*., **42**, 2844–2851.